Eur Radiol (2017) 27:2161–2169
DOI 10.1007/s00330-016-4524-y

EXPERIMENTAL

Abdominal aortic aneurysm follow-up by shear wave elasticity imaging after endovascular repair in a canine model

Antony Bertrand-Grenier[1,2,3,4] · Sophie Lerouge[1,5,6] · An Tang[1,3,7,8,9] · Eli Salloum[1,2,3] · Eric Therasse[1,7,8] · Claude Kauffmann[1,3,7,8] · Hélène Héon[1] · Igor Salazkin[1] · Guy Cloutier[1,2,8,9] · Gilles Soulez[1,3,7,8,9]

Received: 29 December 2015 / Revised: 20 July 2016 / Accepted: 21 July 2016 / Published online: 29 August 2016
© European Society of Radiology 2016

Abstract

Objectives To investigate if shear wave imaging (SWI) can detect endoleaks and characterize thrombus organization in abdominal aortic aneurysms (AAAs) after endovascular aneurysm repair.

Methods Stent grafts (SGs) were implanted in 18 dogs after surgical creation of type I endoleaks (four AAAs), type II endoleaks (13 AAAs) and no endoleaks (one AAA). Color flow Doppler ultrasonography (DUS) and SWI were performed before SG implantation (baseline), on days 7, 30 and 90 after SG implantation, and on the day of the sacrifice (day 180). Angiography, CT scans and macroscopic tissue sections obtained on day 180 were evaluated for the presence, size and type of endoleaks, and thrombi were characterized as fresh or organized. Endoleak areas in aneurysm sacs were identified on SWI by two readers and compared with their appearance on DUS, CT scans and macroscopic examination. Elasticity moduli were calculated in different regions (endoleaks, and fresh and organized thrombi).

Results All 17 endoleaks (100 %) were identified by reader 1, whereas 16 of 17 (94 %) were detected by reader 2. Elasticity moduli in endoleaks, and in areas of organized thrombi and fresh thrombi were 0.2 ± 0.4, 90.0 ± 48.2 and 13.6 ± 4.5 kPa, respectively ($P < 0.001$ between groups). SWI detected endoleaks while DUS (three endoleaks) and CT (one endoleak) did not.

Conclusions SWI has the potential to detect endoleaks and evaluate thrombus organization based on the measurement of elasticity.

Key points

- *SWI has the potential to detect endoleaks in post-EVAR follow-up.*
- *SWI has the potential to characterize thrombus organization in post-EVAR follow-up.*
- *SWI may be combined with DUS in post-EVAR surveillance of endoleak.*

Keywords Abdominal aortic aneurysm · Shear wave elasticity imaging · Endovascular repair · Endoleak · Thrombus

Abbreviations

AAA	Abdominal aortic aneurysm
CEUS	Contrast-enhanced ultrasonography
CI	Confidence interval
CT	Computed tomography

✉ Gilles Soulez
gilles.soulez.chum@ssss.gouv.qc.ca

1 Centre de recherche, Centre hospitalier de l'Université de Montréal (CRCHUM), Montréal, Québec, Canada

2 Laboratoire de biorhéologie et d'ultrasonographie médicale, CRCHUM, Montréal, Québec, Canada

3 Laboratoire clinique de traitement d'images, CRCHUM, Montréal, Québec, Canada

4 Département de physique, Université de Montréal, Montréal, Québec, Canada

5 Laboratoire de biomatériaux endovasculaire, CRCHUM, Montréal, Québec, Canada

6 Département de génie mécanique, École de technologie supérieure, Montréal, Québec, Canada

7 Département de radiologie, Centre hospitalier de l'Université de Montréal (CHUM), Montréal, Québec, Canada

8 Département de radiologie, radio-oncologie et médecine nucléaire, Université de Montréal, Montréal, Québec, Canada

9 Institut de génie biomédical, Université de Montréal, Montréal, Québec, Canada

DSA	Digital subtraction angiography
DUS	Color flow Doppler ultrasonography
EVAR	Endovascular repair
MRI	Magnetic resonance imaging
NIVE	Non-invasive vascular elastography
ROI	Region of interest
SG	Stent graft
SWI	Shear wave imaging
US	Ultrasound

Introduction

Surgical treatment of abdominal aortic aneurysms (AAAs) is increasingly being replaced by endovascular aneurysm repair (EVAR) using stent grafts (SGs) [1]. Persistent blood flow outside the SG and within the aneurysm, called endoleak, is the main EVAR complication that can lead to AAA rupture if not properly detected [2]. The incidence of endoleaks is between 10 % and 30 % [3, 4]. Because endoleaks can develop at any time after EVAR, life-long imaging surveillance is warranted.

Computed tomography (CT), considered to be the gold standard for follow-up after EVAR [5], is able to accurately assess 3D aneurysm morphology and to identify endoleaks. However, CT adds to the cost of EVAR and exposes patients to the risk of nephrotoxicity from the use of contrast agent and the risk of exposure to ionizing radiation even if a lower dose can be given using a single dual-energy CT acquisition in the delayed phase [5–8]. Color flow Doppler ultrasonography (DUS) is increasingly used for imaging after EVAR, but its sensitivity and reproducibility in detecting endoleaks are lower than with CT [9]. Several authors have proposed the use of contrast-enhanced ultrasonography (CEUS) to provide better sensitivity [10–12]. In the absence of rational surveillance protocols targeting those at greatest risk, CEUS is more expensive than DUS for routine observation [13]. CEUS is not recommended for primary surveillance [13]. Three-dimensional CEUS has received renewed interest as it may be more sensitive than two-dimensional CEUS and CT, but there are concerns about its specificity [13, 14]. Given its requirement for the use of intravenous contrast agent, and the longer examination time and greater cost, CEUS has not gained wide acceptance in the clinical setting [15].

Dynamic elastography with shear wave imaging (SWI) technology measures elasticity of the probed tissues in real time [16]. Its originality lies in the fact that it assesses shear wave propagation speed with ultrafast scanning. Since elasticity moduli are related to shear wave speed, color-coded maps can be produced to show quantitative local tissue stiffness in kilopascals. To our knowledge, SWI has never been tested in the context of AAA and EVAR follow-up. Compression elastography has been attempted, but does not provide additional advantages in the detection and classification of endoleaks in comparison with CEUS [17].

This work was supported by the following rationale. Aneurysms without endoleaks should have higher elasticity (Young's) modulus because of more mature thrombus organization. In areas of endoleak, we anticipated that stiffness measurements would be invalid or low because liquid does not support shear motion and hence shear waves cannot propagate in liquid [18]. Hence, we hypothesized that SWI would be able to detect endoleaks and characterize thrombus organization. The goal of this study was to determine if SWI could detect endoleaks and distinguish thrombus organization in AAAs after EVAR in a canine model.

Materials and methods

The institutional Animal Care Committee approved all animal procedures which were performed under general anesthesia in accordance with guidelines of the Canadian Council on Animal Care [19, 20]. Data were acquired between September 2011 and November 2013.

EVAR in a canine model

Fusiform AAAs were created surgically with a venous patch taken from the external jugular vein in 18 mongrel dogs weighing 25 – 50 kg [21, 22]. AAAs were constructed to create endoleaks, with preservation of collateral (lumbar and inferior mesenteric) arteries [21]. SGs were implanted 8 weeks after surgery. Self-expandable SG iliac extensions (Zenith Flex; Cook Medical, Bloomington, IN) were deployed under fluoroscopic guidance to exclude AAAs from flowing blood. Type I endoleaks were created by deploying SGs with a short landing zone (<10 mm), whereas type II endoleaks were created by providing adequate seals at the proximal and distal necks (landing zones ≥15 mm) with retrograde flow from collateral arteries. For a model without endoleaks, collateral (lumbar and inferior mesenteric) arteries were ligated during aneurysm creation, and SGs were implanted with landing ≥15 mm to exclude aneurysms from systemic blood pressure. The initial plan was to create five EVARs with type I endoleaks, seven with type II endoleaks, and six without endoleaks.

The animals were also used to investigate another ultrasound (US) elastography technique: noninvasive vascular elastography (NIVE) [23]. NIVE with the Lagrangian speckle model estimator computes axial and lateral strain as shear maps from radiofrequency US images [24]. The NIVE Lagrangian speckle model estimator algorithm measures deformations induced by natural cardiac pulsations. SWI and NIVE techniques were acquired on separate US units, and the data were processed independently.

Imaging, macroscopic examination, image registration

Dogs were examined by SWI and DUS (Aixplorer, Aix-en-Provence, France) before SG implantation, and at 180 days after EVAR to detect endoleaks. Percutaneous transfemoral angiography was performed to classify endoleaks during SG implantation and before the animals were sacrificed at 180 days. CT was performed and 3 – 5 mm consecutive macroscopic tissue cuts were obtained before and after the animals were sacrificed . Based on the craniocaudal level of axial acquisitions, –the CT scans, DUS acquisitions, macroscopic tissue cuts and SWI were registered and compared. SG position, and aneurysm surface area and diameter in both the macroscopic cuts and the B-mode acquisitions were use as the reference for coregistration with the CT scans.

Angiography

Digital subtraction angiography (DSA; Koordinat 3D II; Siemens, Erlangen, Germany) was performed with serial injections of 20 ml iodine contrast agent at 10 ml/s with a 5 F pigtail positioned first at the level of the suprarenal aorta, then pulled to the aortic bifurcation. Iopamidol 408 mg/ml (Isovue 200; Bracco Diagnostic Canada, Anjou, QC, Canada) was injected for baseline angiography (SG implantation), and iothalamate meglumine 600 mg/ml (Conray 60; Mallinkrodt Canada, Pointe Claire, QC, Canada) was delivered before the animal was sacrificed . Type I endoleaks were defined as opacification of aneurysm sacs from the proximal (type IA) or distal (type IB) neck and outflow through collateral vessels [25]. Type II endoleaks were defined as retrograde aneurysm sac opacification via collateral arteries [25].

B-mode and DUS examinations

All US examinations (SuperSonic, Aixplorer) were performed by a vascular technologist with more than 20 years experience employing a 256-element linear probe (SuperLinear^{TM} SL15-4) at 7.5 MHz. For data acquisition, the technologist performed B-mode US, DUS and SWI in that order and exported the raw data on a separate workstation for NIVE postprocessing. The examination protocol included B-mode acquisition with measurement of AAA maximum diameters and areas in three axial planes at the proximal, middle and distal portions. DUS detected and delineated endoleak areas. Steer angle was first set at 0°, then at 60° right anterior oblique and left anterior oblique. To detect slow-flow endoleaks, the speed range scale was set at 10 cm/s, with smoothing of 0, low wall filter and the high-definition frame rate set to middle.

SWI

SWI was performed after DUS with the same acquisition planes as used for B-mode US and DUS as well as the same probe. SWI parameters were smoothing of 5, opacity of 50 %, and acoustic power as low as reasonably achievable. SWI was analyzed independently by a graduate student (A.B.-G.). The absence of elasticity values within the aneurysm outside the SG with the presence of elasticity values on the posterior wall of the aneurysm sac was defined as an endoleak. Areas without signal and absence of signal beyond were identified and deemed as technical failures. SWI was then registered with the CT scan and macroscopic cuts based on the acquisition level during SWI (proximal, middle or distal aneurysm portion), aneurysm diameter and surface area, including relative SG position. Regions of interest (ROIs) were defined in areas with endoleaks, and fresh and organized thrombi based on the macroscopic cuts. Elasticity moduli were measured using Q-Box. Elastograms were independently reviewed by two readers with 22 years experience in vascular imaging (G.S.) and 10 years experience in abdominal radiology (A.T.). A minimum period of 6 months was retained between the CT scan readings and blinded review of SWI to avoid reading bias by reader 1.

CT scan

CT scans using a 64 detector row scanner (Somatom 64 Sensation; Siemens Medical, Forchheim, Germany) were performed before injection of contrast agent and in the arterial and venous phases after injection of 60 ml iohexol at 4 ml/s (Omnipaque 300 mg I/ml; GE Healthcare, Mississauga, ON, Canada). Prospective gating was done with collimation of 0.6 mm and pitch of 0.2 mm. The diastolic phase was selected based on reconstruction of ten images per cycle, which typically represent 70 % of the cardiac cycle. Parameters were set at 120 kVp and 724 mAs. Endoleak areas were segmented on the arterial or venous phase providing the best opacification and largest area. Two software packages were tested:AquariusNET iNtuition, v. 4.4.7 (TeraRecon, Foster City, CA) for ROI segmentations, and ImageJ, v. 1.47b (National Institutes of Health, Bethesda, MD) for ROI measurements. Endoleak areas were delineated by a graduate student under the supervision of a vascular radiologist (G.S.).

Macroscopic examination

Six months after SG implantation, each dog was killed with a barbiturate overdose (108 mg/kg, euthanyl forte; Bimeda-MTC Animal Health Inc., Cambridge, ON, Canada). Aneurysms were collected and fixed in buffered formalin. The Exakt cutting system (Exakt GmbH, Norderstedt, Germany) generated consecutive macroscopic cuts of 3 –

5 mm, keeping the implant/tissue interface intact. In some samples, the SG was removed and tissues were sent for histology. On stereomicrographs, areas with endoleak-compatible defects were identified, and thrombi were categorized as fresh or organized. Areas of loose thrombi with black or brown coloration were defined as fresh and corresponded mostly to fibrin clots containing red blood cell phantoms and very poor or absent fibrous organization on histology. In contrast, organized thrombi had a dense and yellowish appearance indicating fibrous organization (Fig. 1). Macroscopic slices provided the best correspondence for coregistration with other imaging modalities for each ROI (endoleak, and fresh or organized thrombi).

Endpoint definition

Endoleaks were defined by their presence on CT or DUS and confirmed by a defect in the macroscopic cut at the same level. Endoleak areas on SWI were compared with those seen on DUS, CT and macroscopic cuts. The endoleak surface area ratio corresponded to the mean endoleak areas on the proximal, middle and distal acquisitions expressed as percentages of the total aneurysm surface area. Underestimated areas were considered as less than half the areas measured on the macroscopic cuts. DSA classified endoleaks on the basis of the presence of antegrade or retrograde sacs occurring at the proximal or distal neck (type I endoleaks) or retrograde flow through collateral vessels (type II endoleaks).

Statistical analysis

Statistical analyses were performed with R software (version 3.2.1). The sizes of the endoleaks measured by the different techniques (SWI, DUS, CT and histology) were compared using ANOVA and post-hoc paired *t* tests. Agreement between the two readers for detection of endoleaks by SWI was assessed using Cohen's kappa. Sensitivity and specificity were calculated for endoleak detection by SWI, DUS and CT. The elasticity moduli were determined in different portions of the AAAs (endoleaks, and organized and fresh thrombi) in ROIs. Distributions were assessed for normality. Groups were then compared using the Kruskal-Wallis test with statistical significance set to $P < 0.001$. Finally, for multiple comparisons the Wilcoxon test with Bonferroni correction was used ($P < 0.001$).

Results

No complications occurred during creation of the AAAs, during EVAR or during imaging.

Endpoint censoring

On the basis of the CT scans, DUS and macroscopic cuts combined, four type I endoleaks (one type IA and three type IB), 13 type II endoleaks and one complete seal were observed 6 months after EVAR. One type I endoleak converted into a type II endoleak, and five AAAs targeted for complete seal showed type II endoleaks, most likely because some lumbar arteries were not accessible for ligation. No perigraft collections were observed on the macroscopic slides. Organized thrombi were seen on macroscopic cuts in all 18 dogs, while six AAAs showed fresh thrombi.

Technical failure

Areas deemed to be non-analyzable on SWI (absence of signal on the posterior wall) were estimated to represent 2 % of the accumulated surface area of the SWI acquisitions.

Endoleak detection

Table 1 shows the endoleak areas detected by SWI, DUS and CT at the time the dogs were sacrificed , with the macroscopic cuts serving as the reference (the values shown are the means of the areas traced in the proximal, middle and distal portions of the aneurysms expressed as percentages). The endoleak

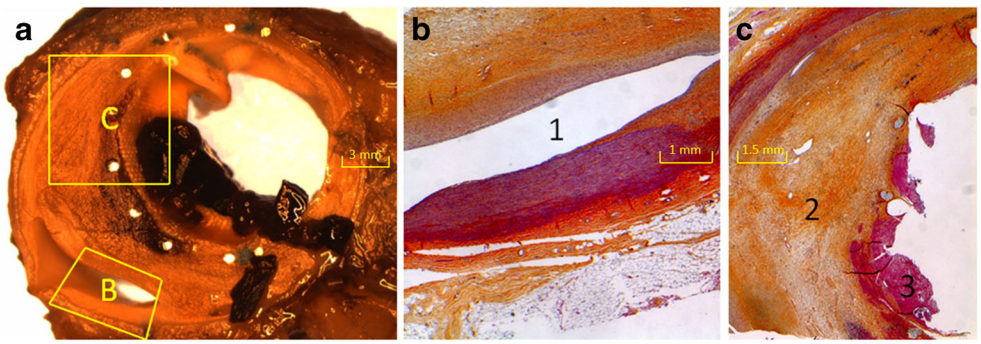

Fig. 1 Macroscopic (**a** 27.3 × 23.5 mm) and histological slides corresponding to the endoleak region (**b** 5.90 × 6.27 mm) and to fresh and organized thrombi (**c** 7.44 × 9.11 mm) with hematoxylin, phloxine and saffron staining. The intraluminal thrombus observed in **a** occurred after death. Zones *1*, *2* and *3* correspond to endoleak, organized thrombus, and fresh thrombus, respectively

Table 1 Endoleak distribution, surface area ratios and detection by different imaging modalities at the time the animals were killed

Dog no.	DUS	SWI[a]	CT	Histology	Endoleak type	Comments
1	11.1 ± 8.6	22.2 ± 6.5	21.6 ± 7.3	13.5 ± 6.6	IB	Detected by all techniques
2	6.2 ± 5.1	21.9 ± 9.2	7.5 ± 1.7	5.5 ± 2.5	II	Detected by all techniques
3	0.3 ± 0.6	17.4 ± 11.3	5.0 ± 2.3	3.1 ± 2.7	II	Underestimated by DUS
4	0.8 ± 1.4	6.1 ± 3.4	0.7 ± 0.9	2.4 ± 1.6	II	Underestimated by DUS and CT
5	8.9 ± 15.4	7.3 ± 10.6	11.2 ± 14.8	3.9 ± 5.6	II	Detected by all techniques, except by reader 2 on SWI
6	0.0 ± 0.0	3.0 ± 2.3	3.1 ± 1.9	1.7 ± 1.7	II	DUS failed
7	4.0 ± 6.6	12.4 ± 9.9	5.2 ± 7.4	4.0 ± 3.5	II	Detected by all techniques
8	4.4 ± 4.9	17.3 ± 3.3	1.0 ± 1.1	6.9 ± 0.3	II	Underestimated by CT
9	1.8 ± 3.2	2.5 ± 4.3	0.0 ± 0.4	1.6 ± 2.8	II	CT failed
10	6.9 ± 10.9	11.6 ± 12.3	8.7 ± 8.4	2.5 ± 1.4	II	Detected by all techniques
11	1.8 ± 1.6	5.5 ± 3.5	2.6 ± 1.8	1.1 ± 1.2	II	Detected by all techniques
12	9.3 ± 16.2	16.2 ± 0.8	11.6 ± 14.8	6.8 ± 8.6	II	Detected by all techniques
13	1.4 ± 2.4	5.0 ± 5.1	0.6 ± 1.0	3.2 ± 2.3	IB	Underestimated by DUS and CT
14	14.2 ± 9.0	18.5 ± 8.6	11.8 ± 14.5	12.4 ± 7.0	IB	Detected by all techniques
15	0.0 ± 0.0	0.0 ± 0.0	0.0 ± 0.0	0.0 ± 0.2	-	No false-positive findings
16	0.0 ± 0.0	2.3 ± 2.6	2.1 ± 3.1	0.9 ± 1.0	IA	DUS failed
17	1.5 ± 2.5	8.3 ± 3.8	3.3 ± 3.9	1.6 ± 1.1	II	Detected by all techniques
18	0.0 ± 0.0	6.3 ± 3.0	1.7 ± 0.8	2.0 ± 1.2	II	DUS failed

The values presented are mean ± SD endoleak surface area ratios on the proximal, middle and distal portions expressed as percentages of the total aneurysm surface areas

DUS color flow Doppler ultrasonography, *SWI* shear wave imaging, *CT* computed tomography

[a] The SWI surface area values were determined by reader 1

areas measured by SWI were significantly different from the areas measured by the other techniques, CT ($P = 0.03$), histology ($P = 0.003$) and DUS ($P = 0.004$). It is possible that SWI overestimated endoleak areas. Histology may have underestimated endoleak areas because of the absence of blood pressure. However, there was no difference in endoleak areas between CT and histology ($P = 0.40$). Reader 1 detected all 17 endoleaks (100 %) and reader 2 missed one endoleak (94 %). There were no false-positive findings. The kappa coefficient was 0.64, which indicates good agreement [26]. Four endoleaks detected by SWI were not revealed by DUS (three endoleaks) or CT (one endoleak; Table 2). Examples of endoleak detection discrepancies with the different imaging modalities are given in Fig. 2 (with underestimation by DUS) and Fig. 3 (CT failed to detect endoleak). The only aneurysm without endoleak was completely sealed on imaging (Fig. 4).

Elasticity modulus measurement

The mechanical properties of endoleaks, and organized and fresh thrombi were significantly different at the time the animals were sacrificed ($P < 0.001$; Fig. 5). As expected, Young's moduli were close to zero (0.2 ± 0.4 kPa, 95 % CI 0.1 – 0.3 kPa) in endoleak areas, and fresh thrombi had lower values (13.6 ± 4.5 kPa, 95 % CI 10.7 – 16.5 kPa) than organized thrombi (90.0 ± 48.2 kPa, 95 % CI 77.0 – 103.0 kPa). We also compared the elasticity moduli of different ROIs in aneurysms that had endoleak types I and II. As shown in Table 3, there were no significant differences in elastic moduli according to endoleak type ($P > 0.5$). Cardiac pulsation and pressure showed no correlation with the elasticity results.

Discussion

This experimental study evaluated SWI as a biomarker of endoleak and thrombus stiffness in a canine model of AAA and endoleaks after SG implantation. AAAs were evaluated in vivo using SWI, DUS, DSA and CT and the findings were correlated with ex vivo findings from macroscopic tissue sections. SWI provides real-time mechanical information on AAA sac contents that is complementary to B-mode and DUS assessments. Our results suggest that the SWI technique following a complete DUS examination may help in detecting slow-flow endoleaks and in thrombus characterization. Since CEUS has also been proposed for monitoring patients after

Table 2 Sensitivity and specificity of imaging methods in the detection of endoleaks

Method	True-positive	False-positive	True-negative	False-negative	Sensitivity (%)	Specificity (%)
DUS	14	0	1	3	82.3	100
SWI						
Reader 1	17	0	1	0	100	100
Reader 2	16	0	1	1	94.1	100
CT	16	0	1	1	94.1	100

DUS color flow Doppler ultrasonography, *SWI* shear wave imaging, *CT* computed tomography

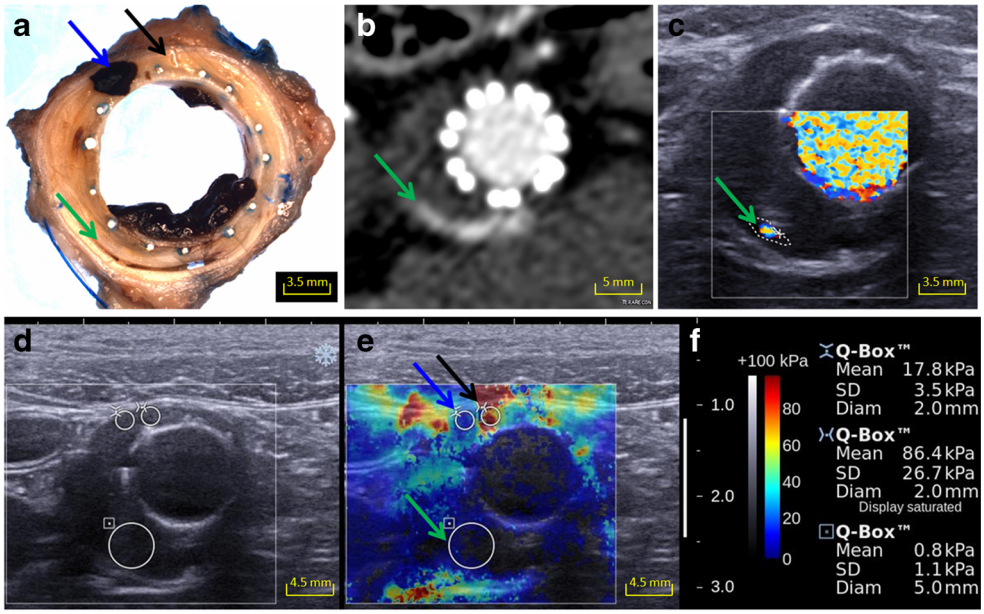

Fig. 2 Characterization of a type II endoleak in dog 3 with axial views obtained using the different techniques where DUS underestimated the endoleak region (*green arrows* endoleak, *blue arrows* fresh thrombus, *black arrows* organized thrombus). **a** Macroscopic cut (27.3 × 23.5 mm). **b** CT image (35 × 35 mm). **c** DUS image (24.4 × 25.9 mm). **d** B-mode US image (38.0 × 32.4 mm). **e** SWI image (38.0 × 32.4 mm). **f** Color scale and Q-Box values for SWI

EVAR [27, 28], a combination of this technique and SWI could reduce the number of CT scans performed for surveillance.

Because liquids do not support shear wave propagation, zones of endoleaks, and even small endoleaks, were mapped near 0 kPa [18]. This provides the opportunity to depict small and/or low-flow endoleaks that are difficult to detect with other techniques [9, 29]. There were no significant differences in stiffness values between type I and II endoleaks. Unlike DUS, shear wave elastography does not depend on flow and is probably more suited to detecting the presence of liquid, which could explain why SWI was able to characterize endoleaks where DUS and CT failed.

SWI cannot differentiate areas containing static fluid as in a sac hygroma from circulating blood as observed in an endoleak. Both areas will display a value of 0 kPa. Therefore, patients with sac hygroma could be falsely diagnosed as positive for endoleak. On the other hand, since sac hygroma is associated with endotension these patients with liquid or soft thrombus need to be followed closely to detect sac expansion [30]. SWI could provide new information about the presence of liquid and endotension for aneurysm surveillance.

SWI is the only current imaging technology that enables the characterization of thrombus stiffness [31]. High stiffness corresponds to organized, solid thrombi, whereas low stiffness corresponds to fresh, soft thrombi. In our study, areas of fresh

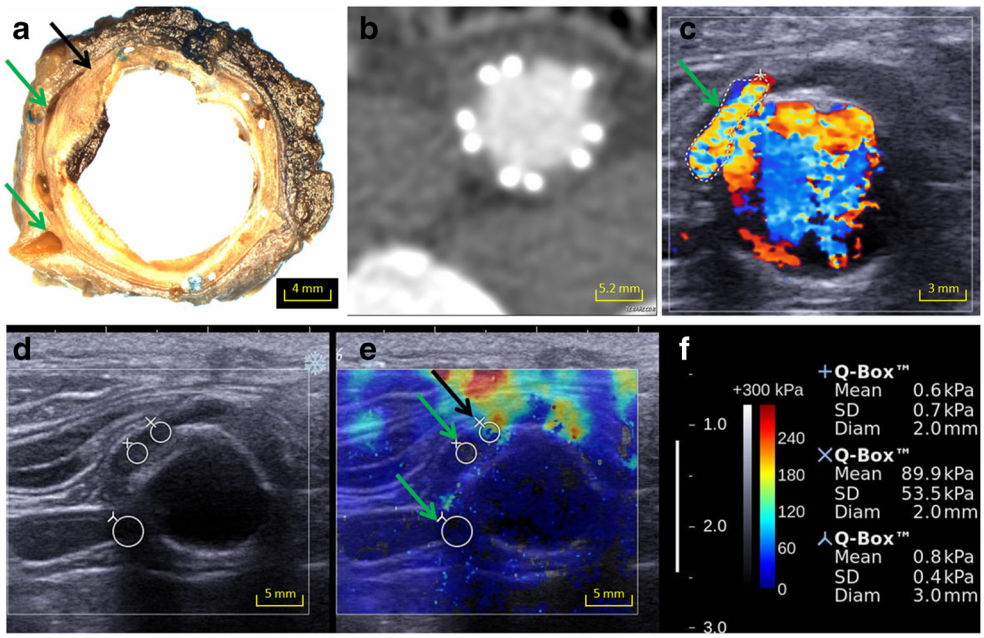

Fig. 3 Characterization of a type II endoleak in dog 9 with axial views obtained using the different techniques where CT failed (*green arrows* endoleak, *black arrows* organized thrombus). **a** Macroscopic cut (23.2 × 20.2 mm). **b** CT image (32 × 32 mm). **c** DUS image (20.7 × 20.3 mm). **d** B-mode US image (32.6 × 30.8 mm). **e** SWI image (32.6 × 30.8 mm). **f** Color scale and Q-Box values for SWI

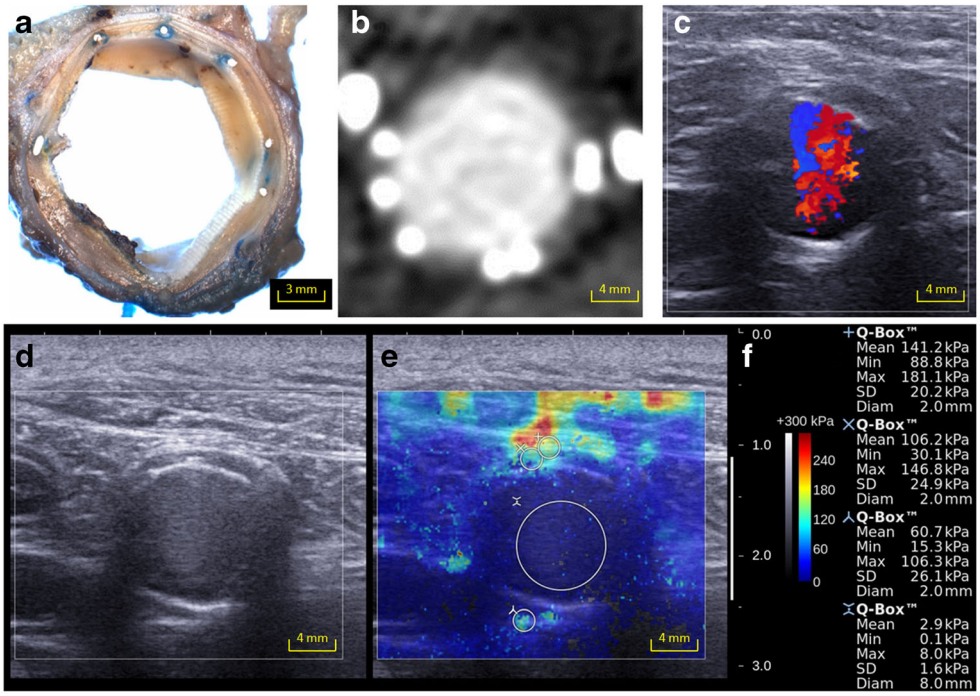

Fig. 4 Characterization of an aneurysm with complete seal in dog 15 with axial views obtained using the different techniques. **a** Macroscopic cut (22.7 × 23.4 mm). **b** CT image (22.6 × 21.9 mm). **c** DUS image (26.9 × 26.5 mm). **d** B-mode US image (31.8 × 31.0 mm). **e** SWI image (31.8 × 31.0 mm). **f** Color scale and Q-Box values for SWI

and organized thrombus areas showed different elasticity moduli. Thus, the technique may allow monitoring of thrombus organization, an important marker of aneurysm healing [32–35]. Also, SWI can characterize fresh thrombi not detectable on CT, thus raising the possibility of depicting fresh thrombi associated with increasing pressure (endotension) in type V endoleaks. Endotension is defined as aneurysm expansion without the presence of endoleaks seen on CT or DUS.

Alternatively, magnetic resonance imaging (MRI) enables detection of endoleaks and characterization of thrombus organization [36–38]. Fresh thrombus areas are more liquid and can be associated with endotension [35]. However, MRI is expensive, less accessible and limited by artefacts related to stent struts, especially from stainless steel SGs [39].

Our study had some limitations. Our aneurysm model was based on venous patch construction, and the pathophysiology of AAA wall degeneration was not reproduced with loss of elastin and vascular smooth muscle cells as well as increased collagen content [40]. In the present work, we did not analyze the mechanical properties of the aortic wall but only the AAA sac contents, which is a realistic approach when compared to clinical reality. Another limitation was that AAA diameters in dogs range from 2 to 3 cm, which is less than in humans. Consequently, we used a high-frequency linear probe (7.5 MHz) to obtain the best compromise in terms of spatial resolution and penetration. This caused some echo losses in the far field and behind SGs. In the clinical setting, low-frequency abdominal probes (range 3.5 to 5 MHz) would be

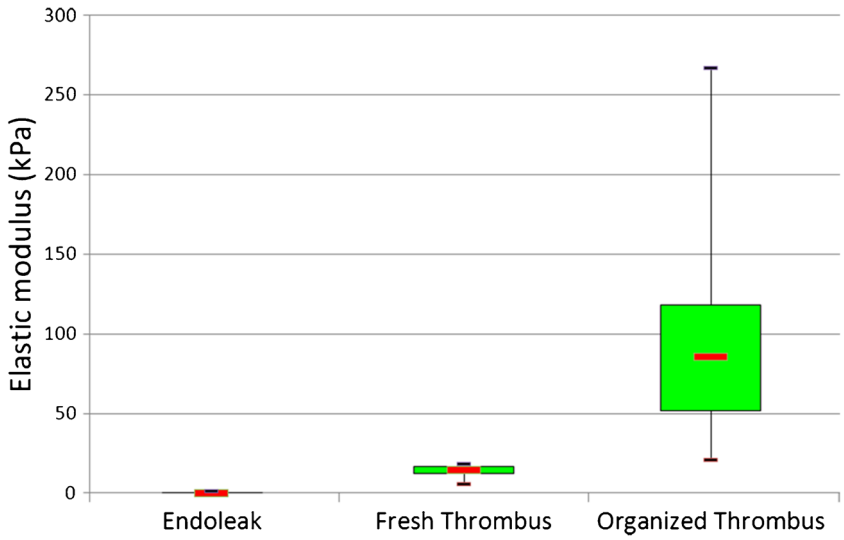

Fig. 5 Elastic moduli of endoleak, fresh thrombus and organized thrombus. The *boxes* indicate quartiles (*red lines* medians), and the *whiskers* extend to the minimum and maximum. The differences in elastic moduli between endoleak, fresh thrombus and organized thrombus are significant ($P < 0.001$)

Table 3 Elasticity moduli of aneurysms ROIs in dogs with type I and type II endoleaks

Aneurysm ROI	Elasticity modulus (kPa)				*P* value
	Type I endoleaks		Type II endoleaks		
	Mean ± SD	95 % CI	Mean ± SD	95 % CI	
Endoleaks	0.3 ± 0.5	0.0 – 0.6	0.2 ± 0.3	0.1 – 0.3	0.59
Fresh thrombi	13.4 ± 4.8	9.2 – 17.6	14.0 ± 4.7	9.4 – 18.6	0.86
Organized thrombi	90.1 ± 45.0	64.6 – 115.6	88.8 ± 51.4	72.5 – 105.1	0.93

required for better penetration. The color scale bar gives visual information on elasticity moduli, but only Q-Box provides actual local stiffness values. For future clinical purposes, data calibration with ROI thresholds adapted to the characterization of AAA sac contents is needed to differentiate thrombus properties in real time.

Another limitation relates to study design. This study was a preclinical feasibility and validation study. Its main objective was to correlate SWI values with AAA sac contents on pathological examination. Thus, we can draw conclusions on the potential of the technology to detect endoleaks and characterize thrombus organization, but assessment of this technique's sensitivity and specificity was limited because of the small sample size, preclinical setting and high incidence of endoleaks (there was only one sealed aneurysm).

In conclusion, this preclinical study confirmed the feasibility of SWI in the follow-up of AAAs after EVAR. The present work illustrates the potential of SWI to detect endoleaks and characterize thrombus organization after EVAR, as indicated by differences in stiffness values. The approach could be combined with DUS surveillance of AAAs after EVAR, which is currently widely practiced to reduce the cost of AAA follow-up and exposure to ionizing radiation and contrast agents [13]. A phase II clinical study is ongoing to evaluate the feasibility and efficacy of SWI with a 3–6-MHz probe to detect endoleaks and correlate thrombus organization with AAA growth or shrinkage in 30 patients [41].

Acknowledgments We are grateful to Jocelyn Lavoie, RT, for preparing and organizing the logistics of this project. We thank Michel Gouin, RT, and Gino Potvin, RT, for their work on US and CT acquisition. We also thank the staff of the CRCHUM animal care facility for their expertise in animal experimentation and follow-up.

The scientific guarantor of this publication is Dr. Gilles Soulez, MD, MSc. The authors declare no relationships with any companies, whose products or services may be related to the subject matter of the article. This study received funding by Fonds de Recherche du Québec – Santé (FRQS) (ARQ no. 22951) and the Canadian Institutes of Health Research (MOP no. 115099). G.S. is supported by a National Scientist award from FRQS. A.T. is supported by a Junior 1 Research Award from the FRQS and Fondation de l'association des radiologistes du Québec (no. 26993). Martin Ladouceur, PhD, kindly provided statistical advice. Institutional Review Board approval and written inform consent were not necessary because the study was an animal study. Approval from the institutional animal care committee was obtained. Some study animals or cohorts have been previously reported as part of an investigation of another elastography technique (non-invasive vascular elastography) [23]. The methodology of this project was experimental.

References

1. Eliason JL, Upchurch GR Jr (2009) Endovascular treatment of aortic aneurysms: state of the art. Curr Treat Options Cardiovasc Med 11(2):136–145
2. Zhou W, Blay E Jr, Varu V et al (2014) Outcome and clinical significance of delayed endoleaks after endovascular aneurysm repair. J Vasc Surg 59(4):915–920
3. van Beek SC, Legemate DA, Vahl A et al (2014) External validation of the Endovascular aneurysm repair Risk Assessment model in predicting survival, reinterventions, and endoleaks after endovascular aneurysm repair. J Vasc Surg 59(6):1555–1561.e3
4. Steingruber IE, Neuhauser B, Seiler R et al (2006) Technical and clinical success of infrarenal endovascular abdominal aortic aneurysm repair: a 10-year single-center experience. Eur J Radiol 59(3):384–392
5. Brown LC, Brown EA, Greenhalgh RM, Powell JT, Thompson SG (2010) Renal function and abdominal aortic aneurysm (AAA): the impact of different management strategies on long-term renal function in the UK EndoVascular Aneurysm Repair (EVAR) Trials. Ann Surg 251(5):966–975
6. Noll RE Jr, Tonnessen BH, Mannava K, Money SR, Sternbergh WC 3rd (2007) Long-term postplacement cost after endovascular aneurysm repair. J Vasc Surg 46(1):9–15, discussion 15
7. White HA, Macdonald S (2010) Estimating risk associated with radiation exposure during follow-up after endovascular aortic repair (EVAR). J Cardiovasc Surg (Torino) 51(1):95–104
8. Müller-Wille R, Borgmann T, Wohlgemuth WA et al (2014) Dual-energy computed tomography after endovascular aortic aneurysm repair: the role of hard plaque imaging for endoleak detection. Eur Radiol 24(10):2449–2457
9. AbuRahma AF, Welch CA, Mullins BB, Dyer B (2005) Computed tomography versus color duplex ultrasound for surveillance of abdominal aortic stent-grafts. J Endovasc Ther 12(5):568–573
10. Giannoni MF, Palombo G, Sbarigia E, Speziale F, Zaccaria A, Fiorani P (2003) Contrast-enhanced ultrasound imaging for aortic stent-graft surveillance. J Endovasc Ther 10:208–217
11. Ten Bosch JA, Rouwet EV, Peters CT et al (2010) Contrast-enhanced ultrasound versus computed tomographic angiography for surveillance of endovascular abdominal aortic aneurysm repair. J Vasc Interv Radiol 21(5):638–643
12. Bendick PJ, Zelenock GB, Bove PG, Long GW, Shanley CJ, Brown OW (2003) Duplex ultrasound imaging with an ultrasound contrast agent: the economic alternative to CT angiography for aortic stent graft surveillance. Vasc Endovasc Surg 37:165–170
13. Karthikesalingam A, Al-Jundi W, Jackson D et al (2012) Systematic review and meta-analysis of duplex ultrasonography, contrast-enhanced ultrasonography or computed tomography for surveillance after endovascular aneurysm repair. Br J Surg 99(11):1514–1523
14. Abbas A, Hansrani V, Sedgwick N, Ghosh J, McCollum CN (2014) 3D contrast enhanced ultrasound for detecting endoleak following endovascular aneurysm repair (EVAR). Eur J Vasc Endovasc Surg 47(5):487–492
15. Wilson SR, Greenbaum LD, Goldberg BB (2009) Contrast-enhanced ultrasound: what is the evidence and what are the obstacles? AJR Am J Roentgenol 193:55–60
16. Sarvazyan AP, Rudenko OV, Swanson SD, Fowlkes JB, Emelianov SY (1998) Shear wave elasticity imaging: a new ultrasonic technology of medical diagnostics. Ultrasound Med Biol 24(9):1419–1435

17. Gürtler VM, Rjosk-Dendorfer D, Reiser M, Clevert DA (2014) Comparison of contrast-enhanced ultrasound and compression elastography in follow-up after endovascular aortic aneurysm repair. Clin Hemorheol Microcirc 57(2):175–183
18. Lerner LS (1996) Modern Physics for Scientists and Engineers, Volume 2. Chapter 22: Summing up. Jones & Bartlett, London, p 622
19. Canadian Council on Animal Care in Science. Available via http://www.ccac.ca/en_/standards/guidelines. Accessed 30 Jul 2016
20. National Research Council of the National Academies (2011) Guide for the care and use of laboratory animals. National Academies Press, Washington DC, Available via https://grants.nih.gov/grants/olaw/Guide-for-the-Care-and-use-of-laboratory-animals.pdf. Accessed 30 Jul 2016
21. Lerouge S, Raymond J, Salazkin I et al (2004) Endovascular aortic aneurysm repair with stent-grafts: experimental models can reproduce endoleaks. J Vasc Interv Radiol 15(9):971–979
22. Soulez G, Lerouge S, Salazkin I, Darsaut T, Oliva VL, Raymond J (2007) Type I and collateral flow in experimental aneurysm models treated with stent-grafts. J Vasc Interv Radiol 18(2):265–272
23. Salloum E, Bertrand-Grenier A, Lerouge S et al (2016) Abdominal aortic aneurysm: follow-up with noninvasive vascular elastography in a canine model. Radiology 279(2):410–419
24. Maurice RL, Ohayon J, Frétigny Y, Bertrand M, Soulez G, Cloutier G (2004) Noninvasive vascular elastography: theoretical framework. IEEE Trans Med Imaging 23(2):164–180
25. Stavropoulos SW, Clark TW, Carpenter JP et al (2005) Use of CT angiography to classify endoleaks after endovascular repair of abdominal aortic aneurysms. J Vasc Interv Radiol 16(5):663–667
26. Cohen J (1960) A coefficient of agreement for nominal scales. Educ Psychol Meas 20(1):37–46
27. Gürtler VM, Sommer WH, Meimarakis G et al (2013) A comparison between contrast-enhanced ultrasound imaging and multislice computed tomography in detecting and classifying endoleaks in the follow-up after endovascular aneurysm repair. J Vasc Surg 58(2):340–345
28. Perini P, Sediri I, Midulla M, Delsart P, Gautier C, Haulon S (2012) Contrast-enhanced ultrasound vs. CT angiography in fenestrated EVAR surveillance: a single-center comparison. J Endovasc Ther 19(5):648–655
29. Elkouri S, Panneton JM, Andrews JC et al (2004) Computed tomography and ultrasound in follow-up of patients after endovascular repair of abdominal aortic aneurysm. Ann Vasc Surg 18(3):271–279
30. Risberg B, Delle M, Lönn L, Syk I (2004) Management of aneurysm sac hygroma. J Endovasc Ther 11(2):191–195
31. Mfoumou E, Tripette J, Blostein M, Cloutier G (2014) Time-dependent hardening of blood clots quantitatively measured in vivo with shear-wave ultrasound imaging in a rabbit model of venous thrombosis. Thromb Res 133(2):265–271
32. Kulcsár Z, Houdart E, Bonafé A et al (2011) Intra-aneurysmal thrombosis as a possible cause of delayed aneurysm rupture after flow-diversion treatment. AJNR Am J Neuroradiol 32(1):20–25
33. Ashton JH, Vande Geest JP, Simon BR, Haskett DG (2009) Compressive mechanical properties of the intraluminal thrombus in abdominal aortic aneurysms and fibrin-based thrombus mimics. J Biomech 42(3):197–201
34. Wang DH, Makaroun M, Webster MW, Vorp DA (2001) Mechanical properties and microstructure of intraluminal thrombus from abdominal aortic aneurysm. J Biomech Eng 123(6):536–539
35. Gasser TC, Görgülü G, Folkesson M, Swedenborg J (2008) Failure properties of intraluminal thrombus in abdominal aortic aneurysm under static and pulsating mechanical loads. J Vasc Surg 48(1):179–188
36. Cornelissen SA, van der Laan MJ, Vincken KL et al (2011) Use of multispectral MRI to monitor aneurysm sac contents after endovascular abdominal aortic aneurysm repair. J Endovasc Ther 18(3):274–279
37. Engellau L, Larsson EM, Albrechtsson U et al (1998) Magnetic resonance imaging and MR angiography of endoluminally treated abdominal aortic aneurysms. Eur J Vasc Endovasc Surg 15(3):212–219
38. Mori K, Saida T, Sato F et al (2016) Endoleak detection after endovascular aneurysm repair using unenhanced MRI with flow suppression technique: feasibility study in comparison with contrast-enhanced CT. Eur Radiol. doi:10.1007/s00330-016-4315-5
39. Weigel S, Tombach B, Maintz D et al (2003) Thoracic aortic stent graft: comparison of contrast-enhanced MR angiography and CT angiography in the follow-up: initial results. Eur Radiol 13(7):1628–1634
40. He CM, Roach MR (1994) The composition and mechanical properties of abdominal aortic aneurysms. J Vasc Surg 20(1):6–13
41. ClinicalTrials.gov (2013) Abdominal aortic aneurysm follow-up after endovascular repair by non-invasive vascular elastography (AAA-Elasto). ClinicalTrials.gov identifier NCT01907386. National Institutes of Health. Available via https://clinicaltrials.gov/ct2/show/NCT01907386?term=abdominal+aortic+aneurysm&recr=Not+yet+recruiting&rslt=Without&type=Intr&titles=abdominal+aortic+aneurysm+followup+after+endovascular+repair+by+noninvasive+vascular+elastography&cntry1=NA%3ACA&state1=NA%3ACA%3AQC&locn=Montreal&rank=1. Accessed 2 Aug 2016